Visco-Elastic Structure Preserving Impedance (VESπ) Control for Compliantly Actuated Robots

Manuel Keppler, Dominic Lakatos, Alexander Werner, Florian Loeffl, Christian Ott and Alin Albu-Schäffer

***Abstract*—In this paper we consider the control of robots that feature visco-elastic actuators with adjustable physical damping. Considering the link variables of the robot as output, the corresponding system dynamics has a relative degree of 3. We present a novel control approach that allows to realize a torque interface on the link side, while preserving the intrinsic visco-elastic structure and the inertial properties of the system. By means of this joint torque interface one can implement link-side position tracking and impedance tasks. For this case, we provide a stability and passivity analysis. The control approach has been verified by experiments with a visco-elastic joint testbed.**

I. Introduction

The reduced model of a flexible joint robot [1] consists of the rigid body dynamics in feedback interconnection with the elastic actuator dynamics. In case that the joint flexibility is caused by parasitic effects like the gear elasticity or the compliance of a joint torque sensor, the joint stiffness usually is quite high and thus the rigid body part gives a good approximation of the dominating dynamics. Several previous control approaches for elastic joint robots consequently started with a control law for the rigid body dynamics and used it as a desired torque to be controlled with the elastic actuator dynamics [2], [3], [4]. Inverse dynamics based control [5] instead allows to design a controller directly for the full flexible robot model without designing first a rigid body controller in an intermediate step. In both cases, the closed loop system can be rendered stably, but will have a significantly different structure than the original open loop behavior.

Starting with [6], [7] we developed a passivity based control framework for elastic joint robots that aims at preserving the intrinsic compliant dynamics. Aiming at a compliance controller, in [7] we utilized a physical interpretation of joint torque feedback as a scaling of motor inertia and implemented the desired compliance on the motor side. While this showed good performance on robots with rather stiff joints, it turned out that for highly elastic robots the vibration damping of the motor side damping in combination with a pure joint torque feedback was not sufficient. In robots with series elastic actuators (SEA) or variable impedance actuators (VIA) one often deliberately incorporates a compliant element in the drive train with a stiffness that is low enough such that the energy storage in the compliant element can be exploited during motion generation [8]. For this type of highly compliant robots, we recently proposed a different control approach that is based on the idea of preserving the structure of the open loop dynamics [9], [10] but, in contract to [7], aims at implementing the damping directly on the link side instead of the motor side. Moreover, in [11] we extended this approach from link side damping to full Cartesian impedance control. While this was analyzed for a SEA in [11], in the present paper we introduce the application of this design idea to a robot with visco-elastic actuators. Despite their similarity in the physical structure, SEA and visco-elastic actuators have quite different control properties. Considering the link side position as an output, the SEA dynamics has a relative degree of 4, while it is at most 3 for a visco-elastic joint [12]. In this paper we will show that the design idea from [11] applied to a visco-elastic actuator in general leads to dynamic state feedback. However, we show that if the generalized elastic force produced by the actuators is a linear function of spring deflections, a tracking control of the link side variables can be achieved, where dynamic feedback can be avoided. A practically relevant advantage of highly compliant visco-elastically actuated systems is the mechanical robustness against external impacts, since the system inherent visco-elastic elements in the power-train act as a low-pass filter on external forces [13]. Thereby, the system does not suffer from bandwidth limitations of any real controller implementation. While the control algorithm of [12] has been validated only in simulation yet, we show by experiments that our approach performs on a real visco-elastic hardware system.

II. Problem Statement

For this work, we consider a reduced model of a n-link robot with visco-elastic joints which is based on the model proposed by Spong in [1], see Fig. 3a. It is given by the following nonlinear differential equations

$$\boldsymbol{M}(\boldsymbol{q})\ddot{\boldsymbol{q}} + \boldsymbol{C}(\dot{\boldsymbol{q}}, \boldsymbol{q})\dot{\boldsymbol{q}} + \boldsymbol{g}(\boldsymbol{q}) = \boldsymbol{\tau}(\dot{\boldsymbol{\theta}}, \boldsymbol{\theta}, \dot{\boldsymbol{q}}, \boldsymbol{q}) + \boldsymbol{\tau}_{ext} \tag{1}$$

$$\boldsymbol{B}\ddot{\boldsymbol{\theta}} + \boldsymbol{\tau}(\dot{\boldsymbol{\theta}}, \boldsymbol{\theta}, \dot{\boldsymbol{q}}, \boldsymbol{q}) = \boldsymbol{u} \tag{2}$$

$$\boldsymbol{\tau}(\dot{\boldsymbol{\theta}}, \boldsymbol{\theta}, \dot{\boldsymbol{q}}, \boldsymbol{q}) = \boldsymbol{D}(t)(\dot{\boldsymbol{\theta}} - \dot{\boldsymbol{q}}) + \boldsymbol{\psi}(\boldsymbol{\theta} - \boldsymbol{q}). \tag{3}$$

Herein, $\boldsymbol{\theta} \in \mathbb{R}^n$ and $\boldsymbol{q} \in \mathbb{R}^n$ represent the motor and link coordinates, respectively.

$\boldsymbol{M} \in \mathbb{R}^{n\times n}$ is the inertia matrix of the rigid links, $\boldsymbol{B} \in \mathbb{R}^{n\times n}$ is the diagonal matrix of the actuator inertias reflected through the respective gearboxes[1]. They have the following properties:

The authors are with the Institute of Robotics and Mechatronics, German Aerospace Center (DLR), 82234 Oberpfaffenhofen, Germany,
web: http://www.dlr.de/rmc/rm/en/staff/manuel.keppler.

Alin Albu-Schäffer is also with Technical University Munich, Chair of Sensor Based Robots and Intelligent Assistance Systems, Department of Informatics, D-85748 Garching, Germany.

[1]More precisely, the motor inertias about their principal axis of rotation are multiplied by the square of the respective gear ratios, see [1] for further details.

Property 1. *The inertia matrices $\boldsymbol{M}(\boldsymbol{q})$ and $\boldsymbol{B}$ are symmetric, positive definite.*

Property 2. *The singular values of $\boldsymbol{M}(\boldsymbol{q})$ and $\boldsymbol{B}$ are bounded from above and bounded from below away from zero, thus both $\boldsymbol{M}^{-1}$ and $\boldsymbol{B}^{-1}$ exist and are bounded.*

These conditions are fulfilled for all pure rotational and pure prismatic joint robots and in some special cases for robots that feature a mix of rotational and prismatic joints, see [14] for an in-depth discussion. We denote the vector of Coriolis and centrifugal forces by $\boldsymbol{C}(\boldsymbol{q},\dot{\boldsymbol{q}})\dot{\boldsymbol{q}}$. Vector $\boldsymbol{g}(\boldsymbol{q})$ represents the gravitational forces. We define $\boldsymbol{C}(\boldsymbol{q},\dot{\boldsymbol{q}})$ via the Christoffel symbols, such that (1) features the following property:

Property 3. *The matrix $\dot{\boldsymbol{M}}(\boldsymbol{q}) - 2\boldsymbol{C}(\boldsymbol{q},\dot{\boldsymbol{q}})$ is skew symmetric for all $(\boldsymbol{q},\dot{\boldsymbol{q}}) \in \mathbb{R}^n \times \mathbb{R}^n$.*

The vector function $\boldsymbol{\tau} : [0,\infty] \times \mathbb{R}^n \times \mathbb{R}^n \times \mathbb{R}^n \times \mathbb{R}^n \to \mathbb{R}^n$ maps the system states to the visco-elastic joint torques that connect the motor with the link side. The first term represents the torques that are due to the adjustable damper. Here, $\boldsymbol{D}(t) \in \mathbb{R}^{n\times n}$ is the diagonal, positive definite joint damping matrix which is assumed to be adjustable and therefor considered to be a function of time t. The second term in (3) represents the torques that are due to the elastic elements. In general, these elastic torques $\boldsymbol{\psi}(\boldsymbol{\phi})$ are a nonlinear function of the spring deflection $\boldsymbol{\phi} = \boldsymbol{\theta} - \boldsymbol{q}$.

Assumption 1. *The elastic torques $\boldsymbol{\psi}(\boldsymbol{\phi})$ are derived from the spring potential function $U_s(\boldsymbol{\phi})$ as follows*

$$\boldsymbol{\psi}(\boldsymbol{\phi}) = \frac{\partial U_s(\boldsymbol{\phi})}{\partial \boldsymbol{\phi}} \in \mathbb{R}^n. \tag{4}$$

The spring potential function is assumed to be positive definite and its Hessian is invertible for all $\boldsymbol{\phi} \in \mathbb{R}^n$.

We denote the local spring stiffness, i.e. the Hessian of the potential function U_s, as

$$\boldsymbol{\kappa}(\boldsymbol{\phi}_0) = \left.\frac{\partial \boldsymbol{\psi}(\boldsymbol{\phi})}{\partial \boldsymbol{\phi}}\right|_{\boldsymbol{\phi}=\boldsymbol{\phi}_0} \in \mathbb{R}^{n\times n}. \tag{5}$$

The dynamics (1)–(3) represent an under-actuated system, where only the motor coordinates $\boldsymbol{\theta}$ can be directly actuated via the motor torques $\boldsymbol{u}\mathbb{R}^n$ which serves as control input. This under-actuation makes control of the link configuration variables a challenging task.

III. Controller Design

Our goal is to provide a torque interface on the link-side of robots with visco-elastic actuation while preserving the visco-elastic structure and inertial properties of the system. To this end we consider the following reference dynamics

$$\boldsymbol{M}(\boldsymbol{q})\ddot{\boldsymbol{q}} + \boldsymbol{C}(\dot{\boldsymbol{q}},\boldsymbol{q}) + \boldsymbol{g}(\boldsymbol{q}) = \boldsymbol{\tau}(\dot{\boldsymbol{\eta}},\boldsymbol{\eta},\dot{\boldsymbol{q}},\boldsymbol{q}) + \boldsymbol{\tau}_i \tag{6}$$

$$\boldsymbol{B}\ddot{\boldsymbol{\eta}} + \boldsymbol{\tau}(\dot{\boldsymbol{\eta}},\boldsymbol{\eta},\dot{\boldsymbol{q}},\boldsymbol{q}) = \bar{\boldsymbol{u}} \tag{7}$$

where $\boldsymbol{\rho},\boldsymbol{\eta} \in \mathbb{R}^n$ are virtual link and motor coordinates of the reference system, respectively. Our new control input is $\bar{\boldsymbol{u}} \in \mathbb{R}^n$. The torques that are due to the visco-elastic actuation are specified by the same function $\boldsymbol{\tau}$ of our original system (3).

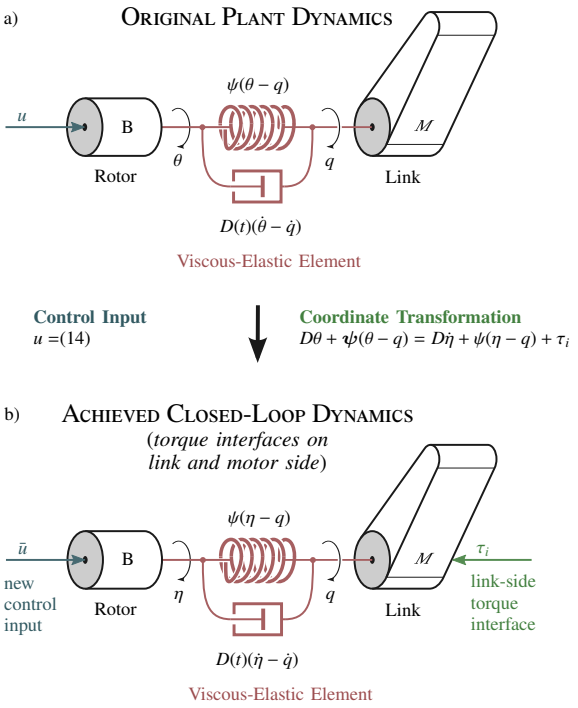

Fig. 1. (a) Graphical representation of a single visco-elastic joint. (b) Achieved closed-loop dynamics with link and motor-side torque interface $\boldsymbol{\tau}_i$ and $\bar{\boldsymbol{u}}$, respectively. (c) Achieved closed-loop dynamics that shows link-side impedance and tracking behavior.

Vector function $\boldsymbol{\tau}_i : \mathbb{R}^n \to \mathbb{R}^n$ represents the torque interface on the link side. Restrictions on $\boldsymbol{\tau}_i$ follow later in this section.

In the following we derive a control input $\boldsymbol{u}$ for our original system such that both systems, i.e. (1)–(2) and (6)–(7), behave equivalently. In particular, we want the links of the original system (1)–(2) to behave identical to the links, of the reference system (6)–(7) with additional torque input. As such, we impose equality of the link coordinates

$$\boldsymbol{\rho}(t) \stackrel{!}{=} \boldsymbol{q}(t) \quad \forall t \in [t_0,\infty), \tag{8}$$

where t_0 represents the starting point in time of our consideration. Our desired dynamics become

$$\boldsymbol{M}(\boldsymbol{q})\ddot{\boldsymbol{q}} + \boldsymbol{C}(\dot{\boldsymbol{q}},\boldsymbol{q}) + \boldsymbol{g}(\boldsymbol{q}) = \boldsymbol{\tau}(\dot{\boldsymbol{\eta}},\boldsymbol{\eta},\dot{\boldsymbol{q}},\boldsymbol{q}) + \boldsymbol{\tau}_i \tag{9}$$

$$\boldsymbol{B}\ddot{\boldsymbol{\eta}} + \boldsymbol{\tau}(\dot{\boldsymbol{\eta}},\boldsymbol{\eta},\dot{\boldsymbol{q}},\boldsymbol{q}) = \bar{\boldsymbol{u}}. \tag{10}$$

We start by imposing equivalence of the link dynamics (1) and (9). To this end we equate the RHS of (1) and (9). This gives us a relation between the original system states $[\dot{\boldsymbol{\theta}},\boldsymbol{\theta},\dot{\boldsymbol{q}},\boldsymbol{q}]$ and the reference system states $[\dot{\boldsymbol{\eta}},\boldsymbol{\eta},\dot{\boldsymbol{q}},\boldsymbol{q}]$ of the form

$$\boldsymbol{\tau}(\dot{\boldsymbol{\theta}},\boldsymbol{\theta},\dot{\boldsymbol{q}},\boldsymbol{q}) = \boldsymbol{\tau}(\dot{\boldsymbol{\eta}},\boldsymbol{\eta},\dot{\boldsymbol{q}},\boldsymbol{q}) + \boldsymbol{\tau}_i(t,\dot{\boldsymbol{q}},\boldsymbol{q}). \tag{11}$$

Under the assumption that (11) can be solved explicitly for $\dot{\boldsymbol{\theta}}$ we can choose $\boldsymbol{\tau}_i$ arbitrarily. It might be even a function of the system states or their higher derivatives. It can also be an explicit function of time. In general this differential relation between the original and reference coordinates cannot be solved analytically for $\boldsymbol{\eta}$. In the following, whenever the knowledge of $\boldsymbol{\eta}$ is required we assume it to be determined by numerical integration of (11). Then, $\dot{\boldsymbol{\eta}}$ follows directly from (11).

A. Control Law Derivation

We derive the coordinate transformation (11) with respect to time and solve for $\ddot{\boldsymbol{\theta}}$. This gives us

$$\ddot{\boldsymbol{\theta}} = \boldsymbol{D}^{-1}\left(\dot{\boldsymbol{\tau}}(\dot{\boldsymbol{\eta}}, \boldsymbol{\eta}, \dot{\boldsymbol{q}}, \boldsymbol{q}) + \dot{\hat{\boldsymbol{\tau}}} - \dot{\boldsymbol{D}}\dot{\boldsymbol{\theta}}\right), \tag{12}$$

where

$$\hat{\boldsymbol{\tau}} = \boldsymbol{D}\dot{\boldsymbol{q}} - \boldsymbol{\psi}(\boldsymbol{\theta} - \boldsymbol{q}) + \boldsymbol{\tau}_i. \tag{13}$$

Next, we substitute (12) in the original system dynamics (1)–(2) and get

$$\boldsymbol{B}\boldsymbol{D}^{-1}\left(\dot{\boldsymbol{\tau}}(\dot{\boldsymbol{\eta}}, \boldsymbol{\eta}, \dot{\boldsymbol{q}}, \boldsymbol{q}) + \dot{\hat{\boldsymbol{\tau}}} - \dot{\boldsymbol{D}}\dot{\boldsymbol{\theta}}\right) + \boldsymbol{\tau}(\dot{\boldsymbol{\eta}}, \boldsymbol{\eta}, \dot{\boldsymbol{q}}, \boldsymbol{q}) + \boldsymbol{\tau}_i = \boldsymbol{u}.$$

We derive the controller in three steps such that the final control law is composed of three terms

$$\boldsymbol{u} = \breve{\boldsymbol{u}} + \hat{\boldsymbol{u}} + \bar{\boldsymbol{u}}. \tag{14}$$

We start with pre-compensating some undesired terms with

$$\breve{\boldsymbol{u}} = \boldsymbol{B}\boldsymbol{D}^{-1}(\dot{\hat{\boldsymbol{\tau}}} - \dot{\boldsymbol{D}}\dot{\boldsymbol{\theta}}) + \boldsymbol{\tau}_i \tag{15}$$

which yields the following intermediary dynamics

$$\dot{\boldsymbol{\tau}}(\dot{\boldsymbol{\eta}}, \boldsymbol{\eta}, \dot{\boldsymbol{q}}, \boldsymbol{q}) + \boldsymbol{D}\boldsymbol{B}^{-1}\boldsymbol{\tau}(\dot{\boldsymbol{\eta}}, \boldsymbol{\eta}, \dot{\boldsymbol{q}}, \boldsymbol{q}) = \boldsymbol{D}\boldsymbol{B}^{-1}(\hat{\boldsymbol{u}} + \bar{\boldsymbol{u}}). \tag{16}$$

Next, we choose $\hat{\boldsymbol{u}}$ such that we achieve equivalence of the motor dynamics (16) and (10). With

$$\hat{\boldsymbol{u}} = \boldsymbol{B}\boldsymbol{D}^{-1}\Big(-\boldsymbol{D}\ddot{\boldsymbol{q}} + \Big(\dot{\boldsymbol{D}} + \boldsymbol{\kappa}(\boldsymbol{\eta} - \boldsymbol{q})\Big)(\dot{\boldsymbol{\eta}} - \dot{\boldsymbol{q}})\Big) + \bar{\boldsymbol{u}} \tag{17}$$

we get for the motor dynamics (2)

$$\boldsymbol{B}\ddot{\boldsymbol{\eta}} + \boldsymbol{\tau}(\dot{\boldsymbol{\eta}}, \boldsymbol{\eta}, \dot{\boldsymbol{q}}, \boldsymbol{q}) = \bar{\boldsymbol{u}}.$$

Thus, we have accomplished our goal of achieving equivalence of the plant dynamics (1)–(2) and our desired dynamics (6)–(10). The link and motor dynamics, respectively, of both systems evolve equally over time.

IV. Link-Side Impedance

In this section we discuss one particularly interesting choice of $\boldsymbol{\tau}_i$. By choosing $\boldsymbol{\tau}_i$ as follows[2]

$$\boldsymbol{\tau}_i(t, \dot{\tilde{\boldsymbol{q}}}, \tilde{\boldsymbol{q}}) = -\boldsymbol{D}_q\dot{\tilde{\boldsymbol{q}}} - \boldsymbol{K}_q\tilde{\boldsymbol{q}} + \boldsymbol{g}(\boldsymbol{q}) + \boldsymbol{M}(t, \tilde{\boldsymbol{q}})\ddot{\boldsymbol{q}}_d + \boldsymbol{C}(t, \dot{\tilde{\boldsymbol{q}}}, \tilde{\boldsymbol{q}})\dot{\boldsymbol{q}}_d \tag{18}$$

with

$$\tilde{\boldsymbol{q}} = \boldsymbol{q} - \boldsymbol{q}_d, \tag{19}$$

we can realize a desired link-side impedance and tracking behavior. The closed-loop link dynamics (9) becomes

$$\boldsymbol{M}(t, \tilde{\boldsymbol{q}})\ddot{\tilde{\boldsymbol{q}}} + \boldsymbol{C}(t, \dot{\tilde{\boldsymbol{q}}}, \tilde{\boldsymbol{q}})\dot{\tilde{\boldsymbol{q}}} + \boldsymbol{D}_q\dot{\tilde{\boldsymbol{q}}} + \boldsymbol{K}_q\tilde{\boldsymbol{q}} = \boldsymbol{\tau}(\dot{\boldsymbol{\eta}}, \boldsymbol{\eta}, \dot{\boldsymbol{q}}, \boldsymbol{q}) \tag{20}$$

$$\boldsymbol{B}\ddot{\boldsymbol{\eta}} + \boldsymbol{\tau}(\dot{\boldsymbol{\eta}}, \boldsymbol{\eta}, \dot{\boldsymbol{q}}, \boldsymbol{q}) = \boldsymbol{0}. \tag{21}$$

Herein, $\boldsymbol{K}_q \in \mathbb{R}^{n\times n}$ is a constant positive definite stiffness matrix. With appropriate choice of matrix $\boldsymbol{D}_q \in \mathbb{R}^{n\times n}$ we can inject a desired link-side damping behavior.

Assumption 2. *The damping matrix $\boldsymbol{D}_q \in \mathbb{R}^n$ can be chosen arbitrarily as long as the corresponding quadratic form $\dot{\tilde{\boldsymbol{q}}}^T\boldsymbol{D}_q\dot{\tilde{\boldsymbol{q}}}$ is positive for any non-zero link-velocity-error vector $\dot{\tilde{\boldsymbol{q}}} \in \mathbb{R}^{n\times n}$.*

Figure 2 shows a graphical representation of the closed-loop dynamics (20) for the single joint case. The multi-joint cased can be imagined as an interconnection of n such elements.

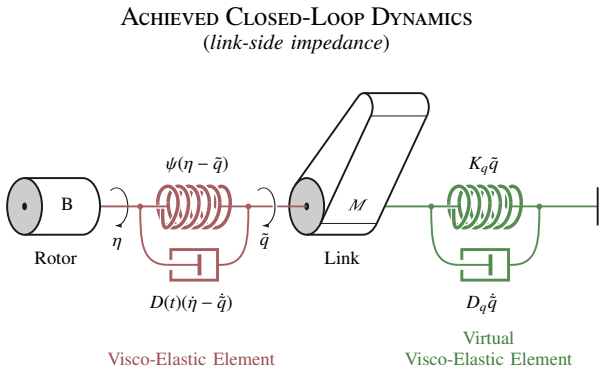

Fig. 2. Achieved closed-loop dynamics that shows link-side impedance and tracking behavior.

V. Avoidance of Dynamic Feedback

An interesting question that may arise when looking at control law $\boldsymbol{u}$ is, whether we can achieve a closed-loop structure with link-side torque interface that is similar to (9)–(10), but without the explicit knowledge of the new motor states $\dot{\boldsymbol{\eta}}, \boldsymbol{\eta}$. As we show in the remainder of this section, this is can at least be done for systems featuring visco-elastic joints with linear-elastic springs. Lets assume, the joint torque in (1)–(2) is of the form

$$\boldsymbol{\tau} = \boldsymbol{D}(t)(\dot{\boldsymbol{\theta}} - \dot{\boldsymbol{q}}) + \boldsymbol{K}(\boldsymbol{\theta} - \boldsymbol{q}), \tag{22}$$

where $\boldsymbol{K} \in \mathbb{R}^{n\times n}$ represents a diagonal, constant and positive definite joint stiffness matrix. Again, we aim to preserve the visco-elastic structure of the system, but this time the coupling torque between link and motor side shall be of the form

$$\bar{\boldsymbol{\tau}} = \boldsymbol{D}_x(t)(\dot{\boldsymbol{\eta}} - \dot{\tilde{\boldsymbol{q}}}) + \boldsymbol{K}(\boldsymbol{\eta} - \tilde{\boldsymbol{q}}), \tag{23}$$

instead of $\boldsymbol{\tau}$, where $\boldsymbol{D}_x$ represents a diagonal, possibly time-variant damping matrix. A discussion of $\boldsymbol{D}_x$ is given in at the end of this section. Our desired link dynamics is of the form

$$\boldsymbol{M}(\boldsymbol{q})\ddot{\boldsymbol{q}} + \boldsymbol{C}(\dot{\boldsymbol{q}}, \boldsymbol{q})\dot{\boldsymbol{q}} + \boldsymbol{g}(\boldsymbol{q}) = \bar{\boldsymbol{\tau}} + \boldsymbol{\tau}_i, \tag{24}$$

where $\bar{\boldsymbol{\tau}}$ shall now be the coupling torque between the link and motor side. The link-side torque interface is again represented by $\boldsymbol{\tau}_i$. By forcing equivalence of the original link dynamics (1) and our desired link dynamics (24) we get the following relation between the old and new system states

$$\boldsymbol{\tau}(\dot{\boldsymbol{\theta}}, \boldsymbol{\theta}, \dot{\boldsymbol{q}}, \boldsymbol{q}) = \bar{\boldsymbol{\tau}}(\dot{\boldsymbol{\eta}}, \boldsymbol{\eta}, \dot{\tilde{\boldsymbol{q}}}, \tilde{\boldsymbol{q}}) + \boldsymbol{\tau}_i. \tag{25}$$

We now proceed analogously to Sec. III. We derive (25) with respect to time and solve for $\ddot{\boldsymbol{\theta}}$

$$\ddot{\boldsymbol{\theta}} = \boldsymbol{D}^{-1}(\dot{\bar{\boldsymbol{\tau}}} + \dot{\hat{\boldsymbol{\tau}}} - \dot{\boldsymbol{D}}\dot{\boldsymbol{\theta}}). \tag{26}$$

Substitution of (26) in the original motor dynamics (2) gives

$$\boldsymbol{B}\boldsymbol{D}^{-1}(\dot{\bar{\boldsymbol{\tau}}} + \dot{\hat{\boldsymbol{\tau}}} + \dot{\boldsymbol{D}}\dot{\boldsymbol{\theta}}) + \bar{\boldsymbol{\tau}} + \boldsymbol{\tau}_i = \boldsymbol{u}.$$

[2] We use the following abbreviations: $\boldsymbol{M}(t, \tilde{\boldsymbol{q}}) = \boldsymbol{M}(\boldsymbol{q} - \boldsymbol{q}_d(t))$ and $\boldsymbol{C}(t, \dot{\tilde{\boldsymbol{q}}}, \tilde{\boldsymbol{q}}) = \boldsymbol{C}(\dot{\boldsymbol{q}} - \dot{\boldsymbol{q}}_d(t), \boldsymbol{q} - \boldsymbol{q}_d(t))$

Again, we derive our control input $\boldsymbol{u}$ in three steps such that the resulting control law is composed of three terms

$$\boldsymbol{u} = \check{\boldsymbol{u}}_{adf} + \hat{\boldsymbol{u}}_{adf} + \bar{\boldsymbol{u}}_{adf}. \tag{27}$$

Choosing

$$\check{\boldsymbol{u}}_{adf} = \boldsymbol{B}\boldsymbol{D}^{-1}\left(\dot{\hat{\boldsymbol{\tau}}} + \dot{\boldsymbol{D}}\dot{\boldsymbol{\theta}}\right) + \boldsymbol{\tau}_i \tag{28}$$

results in the following intermediary dynamics

$$\dot{\bar{\boldsymbol{\tau}}}(\dot{\boldsymbol{\eta}}, \boldsymbol{\eta}, \dot{\boldsymbol{q}}, \boldsymbol{q}) + \boldsymbol{D}\boldsymbol{B}^{-1}\bar{\boldsymbol{\tau}}(\dot{\boldsymbol{\eta}}, \boldsymbol{\eta}, \dot{\boldsymbol{q}}, \boldsymbol{q}) = \boldsymbol{D}\boldsymbol{B}^{-1}(\hat{\boldsymbol{u}}_{adf} + \bar{\boldsymbol{u}}_{adf}). \tag{29}$$

Next, we choose

$$\hat{\boldsymbol{u}}_{adf} = \boldsymbol{B}\boldsymbol{D}^{-1}\frac{\mathrm{d}}{\mathrm{dt}}\left(-\boldsymbol{D}_x\dot{\tilde{\boldsymbol{q}}} - \boldsymbol{K}_x\tilde{\boldsymbol{q}}\right) \tag{30}$$

which yields

$$\boldsymbol{B}\ddot{\boldsymbol{\eta}} + \boldsymbol{D}_{\boldsymbol{\eta}}\dot{\boldsymbol{\eta}} + \boldsymbol{D}_x^{-1}\boldsymbol{D}\bar{\boldsymbol{\tau}} = \boldsymbol{D}_x^{-1}\boldsymbol{D}\bar{\boldsymbol{u}}_{adf},$$

where $\boldsymbol{D}_{\boldsymbol{\eta}} = \boldsymbol{B}\boldsymbol{D}_x^{-1}\left(\dot{\boldsymbol{D}}_x + \boldsymbol{K}\right)$. Last, we shape the time-variant motor inertia to the constant inertia $\boldsymbol{B}$ with

$$\bar{\boldsymbol{u}} = (\boldsymbol{I} - \boldsymbol{D}^{-1}\boldsymbol{D}_x)\bar{\boldsymbol{\tau}}. \tag{31}$$

This results in the final motor dynamics

$$\boldsymbol{B}\ddot{\boldsymbol{\eta}} + \boldsymbol{D}_{\boldsymbol{\eta}}\dot{\boldsymbol{\eta}} + \bar{\boldsymbol{\tau}} = \boldsymbol{0}. \tag{32}$$

Compared to (10) we have an additional damper term that purely acts on the motor inertia $\boldsymbol{B}$.

Assumption 3. *The damping matrix $\boldsymbol{D}_x$ has to satisfy the same assumptions as $\boldsymbol{D}$. But in addition, one has to ensure that the quadratic form $\dot{\boldsymbol{\eta}}^T\left(\dot{\boldsymbol{D}}_x + \boldsymbol{K}\right)\dot{\boldsymbol{\eta}}$ is always positive for nonzero velocity vectors $\dot{\boldsymbol{\eta}}$. One sufficient condition would be, that the minimum local stiffness values $\boldsymbol{\kappa}_{i,i}$ have to be greater than the corresponding rates of decrease of the elements $\boldsymbol{D}_{x_{i,i}}$.*

Remark 1. This means, as long as $\boldsymbol{D}$ changes sufficiently slow, i.e. the local stiffness values are greater than the corresponding rates of decrease of $\boldsymbol{D}$, we can set $\boldsymbol{D}_x$ equal to $\boldsymbol{D}$. In this case we would fully preserve the original visco-elastic element for closed-loop dynamics.

VI. Passivity Analysis

In this section, we analyze the passivity properties of the closed-loop systems (20)–(21). The physically motivated design approach of the reference dynamics, c.f. Fig. 3, motivates the following intuitive storage functions

$$S_q(\dot{\tilde{\boldsymbol{q}}}, \tilde{\boldsymbol{q}}) = \frac{1}{2}\dot{\tilde{\boldsymbol{q}}}^{\mathrm{T}}\boldsymbol{M}(t, \tilde{\boldsymbol{q}})\dot{\tilde{\boldsymbol{q}}} + U_q(\tilde{\boldsymbol{q}}), \tag{33}$$

$$S_\eta(\dot{\boldsymbol{\eta}}, \boldsymbol{\eta}, \tilde{\boldsymbol{q}}) = \frac{1}{2}\dot{\boldsymbol{\eta}}^{\mathrm{T}}\boldsymbol{B}\dot{\boldsymbol{\eta}} + U_s(\boldsymbol{\eta} - \tilde{\boldsymbol{q}}). \tag{34}$$

The sum $S = S_q + S_\eta$ comprises the total virtual energy of the closed-loop system (20)–(21). By virtue of Prop. 3, the time derivative of the storage function, expressed along the solutions of the closed-loop dynamics, gives

$$\dot{S}_q(\dot{\tilde{\boldsymbol{q}}}, \tilde{\boldsymbol{q}}) = -\dot{\tilde{\boldsymbol{q}}}^{\mathrm{T}}\boldsymbol{D}\dot{\tilde{\boldsymbol{q}}} + \dot{\tilde{\boldsymbol{q}}}^{\mathrm{T}}\psi(\boldsymbol{\eta} - \tilde{\boldsymbol{q}}) + \dot{\tilde{\boldsymbol{q}}}^{\mathrm{T}}\boldsymbol{\tau}_{ext},$$
$$\dot{S}_\eta(\dot{\boldsymbol{\eta}}, \boldsymbol{\eta}, \tilde{\boldsymbol{q}}) = -\dot{\boldsymbol{\eta}}^{\mathrm{T}}\boldsymbol{K}_d\dot{\boldsymbol{\eta}} - \dot{\tilde{\boldsymbol{q}}}^{\mathrm{T}}\psi(\boldsymbol{\eta} - \tilde{\boldsymbol{q}}).$$

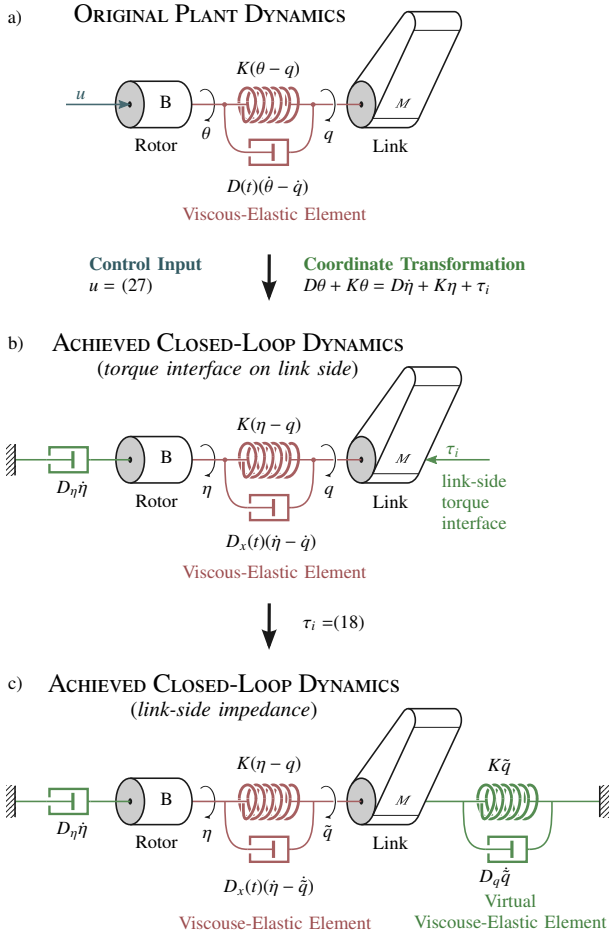

Fig. 3. Graphical representation of the achieved closed-loop behaviors on the basis of a single viscous-elastic joint as depicted in (a). (b) Added link-side torque interface $\boldsymbol{\tau}_i$. (c) Achieved closed-loop dynamics that shows link-side impedance and tracking behavior.

We can identify three kind of terms. First, the term $\dot{\boldsymbol{q}}^{\mathrm{T}}\psi(\boldsymbol{q}-\boldsymbol{\eta})$ corresponds to an interconnection port between the motor and link dynamics. Second, $\dot{\tilde{\boldsymbol{q}}}^{\mathrm{T}}\boldsymbol{\tau}_{ext}$ represents an interconnection port that allows energy exchange between the robot and its environment. Third, we have terms that correspond to the power dissipation that is due to dampers. The result so far motivate the following proposition:

Proposition 1. *The closed-loop system* (20)–(21) *represents a passive map from external forces $\boldsymbol{\tau}_{ext}$ to the velocities $\dot{\tilde{\boldsymbol{q}}}$.*

Proof. The time derivative of the storage functions S, expressed along the solution of (20)–(21), is given by

$$\begin{aligned}\dot{S}(\dot{\boldsymbol{\eta}}, \boldsymbol{\eta}, \dot{\tilde{\boldsymbol{q}}}, \tilde{\boldsymbol{q}}) = &-\dot{\tilde{\boldsymbol{q}}}^{\mathrm{T}}\boldsymbol{D}_q\dot{\tilde{\boldsymbol{q}}} - (\dot{\boldsymbol{\theta}}^{\mathrm{T}} - \dot{\tilde{\boldsymbol{q}}}^{\mathrm{T}})\boldsymbol{D}_{\boldsymbol{\eta}}(\dot{\boldsymbol{\theta}} - \dot{\tilde{\boldsymbol{q}}}) \\ &+ \dot{\tilde{\boldsymbol{q}}}^{\mathrm{T}}\boldsymbol{\tau}_{ext} \leq \dot{\tilde{\boldsymbol{q}}}^{\mathrm{T}}\boldsymbol{\tau}_{ext}.\end{aligned} \tag{35}$$

which completes the proof. □

The storage function S allows us to make an analog statement for the closed-loop dynamics (18),(24),(32).

Proposition 2. *The closed-loop system* (18),(24),(32) *represents a passive map from the external torques $\boldsymbol{\tau}_{ext}$ to the velocities $\dot{\tilde{\boldsymbol{q}}}$.*

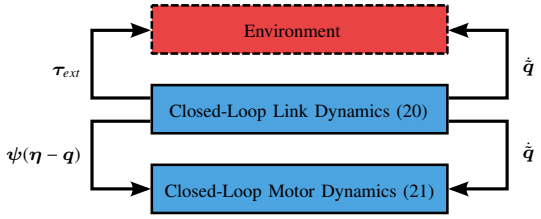

Fig. 4. Passivity properties of the closed-loop dynamics (20)–(21).

Proof. The time derivative of the storage functions S, expressed along the solution of (20)–(21), is given by

$$\begin{aligned}\dot{S}(\dot{\eta}, \dot{\eta}, \dot{\tilde{q}}, \tilde{q}) = &- \dot{\tilde{q}}^{\mathrm{T}} \boldsymbol{D}_q \dot{\tilde{q}} - (\dot{\eta}^{\mathrm{T}} - \dot{\tilde{q}}^{\mathrm{T}}) \boldsymbol{D}_\eta (\dot{\eta} - \dot{\tilde{q}}) \\ &- \dot{\eta}^{\mathrm{T}} \boldsymbol{D}_\eta \dot{\eta} + \dot{\tilde{q}}^{\mathrm{T}} \tau_{ext} \leq \dot{\tilde{q}}^{\mathrm{T}} \tau_{ext}.\end{aligned} \tag{36}$$

which completes the proof. □

VII. Stability Analysis

In this section we present a formal stability analysis of the closed-loop systems (20)–(21) for the free motion case, i.e. in absence of external generalized forces.

Under consideration of Assumptions 1, we obtain the following unique equilibrium point of the closed-loop system (20)–(21)

$$\{\dot{\eta} = \mathbf{0},\ \eta = \tilde{q},\ \dot{\tilde{q}} = \mathbf{0},\ \tilde{q} = \mathbf{0}\}. \tag{37}$$

The time derivative of the storage function S, cf. (35), motivates the following proposition.

Proposition 3. *Consider the closed-loop dynamics* (20)–(21) *in absence of external forces τ_{ext}. The equilibrium point* (37)*, is globally uniformly stable. The velocities $\dot{\tilde{q}}$ and $\dot{\eta}$ converge to the origin as $t \to \infty$.*

Proof. We invoke Lyapunov's direct method for non-autonomous systems [15] to show stability. Consider

$$V(t, \dot{\eta}, \eta, \dot{\tilde{q}}, \tilde{q}) = S(t, \dot{\eta}, \eta, \dot{\tilde{q}}, \tilde{q}) \tag{38}$$

as Lyapunov function candidate. The positive definiteness follows directly from the assumptions made in Sec. II. The time derivative of V along the solutions of (20)–(21) is given by

$$\dot{V}(t, \dot{\eta}, \eta, \dot{\tilde{q}}, \tilde{q}) = -\dot{\tilde{q}}^{\mathrm{T}} \boldsymbol{D}_q \dot{\tilde{q}} - (\dot{\eta}^{\mathrm{T}} - \dot{\tilde{q}}^{\mathrm{T}}) \boldsymbol{D}(t)(\dot{\eta} - \dot{\tilde{q}})$$

which is a negative semi-definite function. Thus, (38) qualifies as Lyapunov function. In order to extent the statement of statement of stability to global uniform stability we have to show the existence of a time-invariant upper bound V^* s.t. $V^*(\dot{\eta}, \eta, \dot{\tilde{q}}, \tilde{q}) \geq 0$. To this end, consider the following upper

$$V^*(\dot{\eta}, \eta, \dot{\tilde{q}}, \tilde{q}) = \frac{1}{2}\bar{M}\|\dot{\tilde{q}}\|^2 + \frac{1}{2}\dot{\eta}^{\mathrm{T}} \boldsymbol{B} \dot{\eta} + U_q(\tilde{q}) + U_s(\eta - \tilde{q})$$

which satisfies the condition. Herein, $\bar{M} \in \mathbb{R}$ is defined as follows

$$\bar{M} := \max_{t \in \mathbb{R}^+, \tilde{q} \in \mathbb{R}^n} \sigma(\boldsymbol{M}(t, \tilde{q})).$$

Under the assumptions made in Sec. II the existence of $\bar{M}$ is ensured [14].

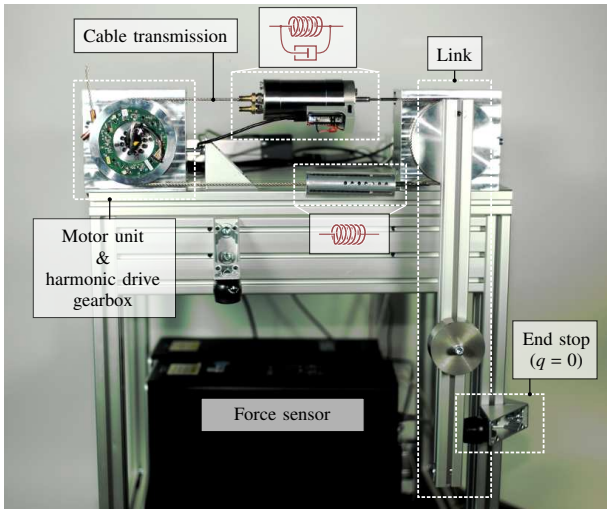

Fig. 5. Experimental setup with motor unit (left), link (right) connected by the coupling mechanism (middle).

In order to show converges of the velocities, i.e. $\dot{\tilde{q}} \to \mathbf{0}$ and $\dot{\eta} \to \mathbf{0}$ as $t \to \infty$, we invoke Barbalat's Lemma [16]. In order to apply Barbalat's Lemma we have yet to show the $\dot{V}(t, \dot{\eta}, \eta, \dot{\tilde{q}}, \tilde{q})$ is uniformly continuous in time. For that it is sufficient to proof the boundedness of $\ddot{V}$, see [17]. The second time derivative of V along the solutions of (20)–(21) is given by

$$\begin{aligned}\ddot{V}(t, \dot{\eta}, \eta, \dot{\tilde{q}}, \tilde{q}) = &- \dot{\tilde{q}}^{\mathrm{T}} \boldsymbol{D}_q \ddot{\tilde{q}} - (\dot{\eta}^{\mathrm{T}} - \dot{\tilde{q}}^{\mathrm{T}}) \boldsymbol{D}(t)(\ddot{\eta} - \ddot{\tilde{q}}) \\ &- (\dot{\eta}^{\mathrm{T}} - \dot{\tilde{q}}^{\mathrm{T}}) \dot{\boldsymbol{D}}(t)(\dot{\eta} - \dot{\tilde{q}})\end{aligned}$$

Above we have shown already stability of the closed-loop dynamics (20)–(21). With this in mind, and under consideration of Prop. 1, we can directly conclude the boundedness of $\ddot{\eta}$ and $\ddot{\tilde{q}}$ and thus the boundedness of $\ddot{V}$. This means, all conditions of Barbalat's Lemma are satisfied which suggests that $\dot{V} \to 0$ for $t \to \infty$. Considering (38) allows us to conclude converges of the velocities $\dot{\eta}$ and $\dot{\tilde{q}}$ to the origin. □

In analog fashion we make a similar statement for the closed-loop dynamics (18),(24),(32).

Proposition 4. *Consider the closed-loop dynamics* (18),(24),(32) *in absence of external forces τ_{ext}. The equilibrium point* (37)*, is globally uniformly stable. The velocities $\dot{\tilde{q}}$ and $\dot{\eta}$ converge to the origin as $t \to \infty$.*

Proof. We can use the same Lyapunov function from above, (38), and proceed analogously. □

VIII. Experiments

To evaluate the performance of the control approach, two experiments are conducted. In this section the experimental setup is described followed by an analysis of the tracking performance for a step response and a chirp signal.

The experimental setup is shown in Fig. 5. It consists of three main components, the motor unit on the left hand side, the link inertia on the right hand side and the coupling mechanism in between. The drive component in use is a repurposed LWR robot drive with a harmonic drive gear, a rotary

TABLE I
SYSTEM PARAMETERS OF THE TESTBED

Parameter	Symbol	Value	Unit
Link-side inertia	$\boldsymbol{M}$	0.45	kg m^2
Motor-side inertia	$\boldsymbol{B}$	1.53	kg m^2
Joint stiffness	$\boldsymbol{K}$	350	N m rad^{-1}
Joint damping	$\boldsymbol{D}$	31	N m rad^{-1} s
Motor torque ($\boldsymbol{u}$) limits	–	±100	N m

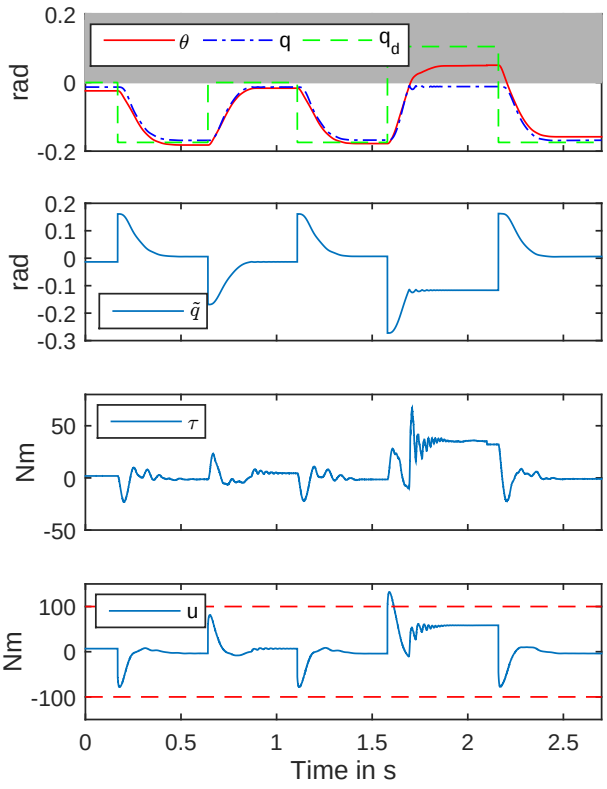

Fig. 6. Experimental results for a sequence of steps in the desired link position q_d. First: system states θ, q and desired position q_d. The grey areas illustrates the position of the end stop. Second: control error $\tilde{q}$. Third: the torque in the visco-elastic element τ as measured by the torque sensor of the drive unit. Forth: control input u with the limits denoted as red dashed lines.

encoder and a torque sensor. A rigid beam, together with a rotary encoder and an external force sensor, constitute the link side inertia. The link and motor side are connected by two antagonistic tendons. In the upper tendon a novel viscoelastic element is integrated, the lower contains only a steel spring.

The viscoelastic element itself is composed of two counteracting air springs and an adjustable hydraulic damper. The combination of the non-linear air springs allow a near-linear stiffness characteristic. Table I displays the essential numeric values.

The step response experiment shown in Fig. 6 contains a sequence of five steps. All but the forth step move the link to positions in free space. The forth step drives the link into the end stop at $q = 0$. This results in a saturation of the motor torque and a non-zero static error. The motor can provide a maximum torque of ± 100 N m.

Fig. 7 shows the tracking performance for a chirp reference signal that rises from 1 to 5 Hz. The performance is

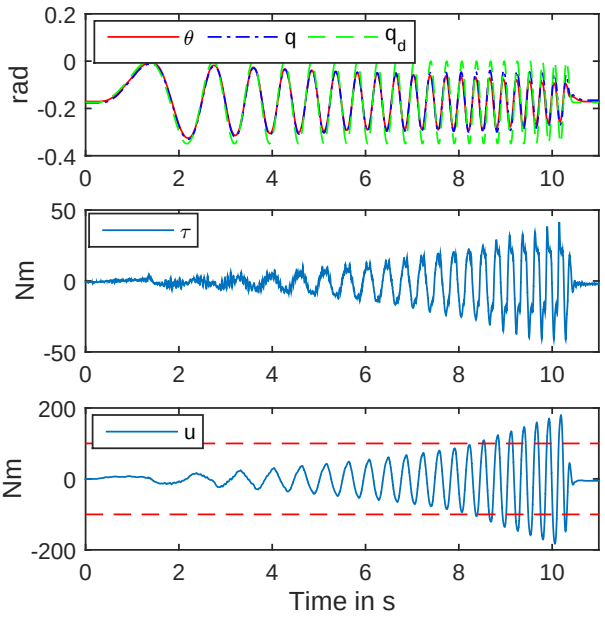

Fig. 7. Experimental results for a chirp signal. Top: system states and desired position q_d. Middle: link torque τ. Bottom: system input u with the limits denoted as red dashed lines.

degraded by the presence of significant coulomb friction in the viscoelastic element which will be reduced in the future. As expected, the performance further degrades when the system input saturates.

Interestingly, the controller remains stable even it situations where the control input saturates, c.f the impact phase of the first experiment and chirp experiment.

IX. SUMMARY AND CONCLUSIONS

In this paper we presented a novel control approach for robots with visco-elastic joints. The main design idea is to render the closed loop dynamics such that a desired virtual joint torque is acting on the link side, while the intrinsic visco-elastic joint dynamics is preserved. By means of this virtual joint torque one can implement position tracking and impedance tasks. An important aspect of this controller design is the fact that the desired modification of the effective link side dynamics requires a change of coordinates on the motor side, leading to a virtual motor coordinate $\boldsymbol{\eta}$. In our previous work [11] this design approach was already analyzed for robots with series-elastic actuators without joint damping. The additional damping in visco-elastic joints has the important consequence that, in general, the virtual motor coordinate cannot be directly computed any more by a simple state transformation, but has to be integrated over time. The controller thus becomes a dynamic state feedback, in contrast to the static state feedback in [11]. We also show that by a modification of the controller this dynamic feedback can be avoided if one allows a digress from the intrinsic visco-elastic joint dynamics. In addition to a stability and passivity analysis, the control approach was also verified by preliminary experiments with a single visco-elastic joint.

Appendix

If we had stopped our controller design at (16) we would have achieved a closed-loop dynamics with decoupled torque error dynamics. By introducing a new state variable $\tilde{\boldsymbol{\tau}} \in \mathbb{R}^n$ and replacing $\boldsymbol{\tau}(\dot{\boldsymbol{\eta}}, \boldsymbol{\eta}, \dot{\tilde{\boldsymbol{q}}}, \tilde{\boldsymbol{q}})$ with $\tilde{\boldsymbol{\tau}}$ in the coordinate transformation (11) we get after rearranging some terms

$$\tilde{\boldsymbol{\tau}} = \boldsymbol{\tau}(\dot{\boldsymbol{\theta}}, \boldsymbol{\theta}, \dot{\boldsymbol{q}}, \boldsymbol{q}) - \boldsymbol{\tau}_i. \tag{39}$$

As such, $\tilde{\boldsymbol{\tau}}$ can be interpreted as the torque error between the real physical torque $\boldsymbol{\tau}(\dot{\boldsymbol{\theta}}, \boldsymbol{\theta}, \dot{\boldsymbol{q}}, \boldsymbol{q})$ and the desired link-side torque $\boldsymbol{\tau}_i$. Substituting $\boldsymbol{\tau}(\dot{\boldsymbol{\eta}}, \boldsymbol{\eta}, \dot{\boldsymbol{q}}, \boldsymbol{q})$ with $\tilde{\boldsymbol{\tau}}$ in (16) we get

$$\dot{\tilde{\boldsymbol{\tau}}} + \boldsymbol{D}\boldsymbol{B}^{-1}\tilde{\boldsymbol{\tau}} = \boldsymbol{D}\boldsymbol{B}^{-1}(\hat{\boldsymbol{u}} + \bar{\boldsymbol{u}}). \tag{40}$$

By choosing $\hat{\boldsymbol{u}} = \bar{\boldsymbol{u}} = \boldsymbol{0}$ we would get a decoupled torque-error dynamics that converges exponentially to zero. The converges rate is determined by entries of the inertia matrices and diagonal damping $\boldsymbol{B}$ and $\boldsymbol{D}$, respectively. The total control input $\boldsymbol{u}_1$ would ultimately reduce to

$$\boldsymbol{u} = \check{\boldsymbol{u}} \tag{41}$$

and we get the following torque error dynamics.

$$\dot{\tilde{\boldsymbol{\tau}}} + \boldsymbol{D}\boldsymbol{B}^{-1}\tilde{\boldsymbol{\tau}} = \boldsymbol{0}. \tag{42}$$

This results in a control law with 'smart' gain selection as all 'gain matrices in front of the state feedback terms in $\boldsymbol{u}_1$ are determined by the system properties. The gain selection can be considered 'smart' in some sense as the convergence rate of the torque errors $\tilde{\boldsymbol{\tau}}_i$ decreases with increasing motor inertia $\boldsymbol{B}_{i,i}$ and it decreases with increasing damping values $\boldsymbol{D}_{i,i}$. This kind of control performance trend is precisely as one would expect. Clearly, lower motor inertia lead to higher motor accelerations. Higher damping values increase the joint torque bandwidth. Both effects eventually should lead to increased control performance, i.e. faster convergence of the torque. If the user wishes to set the convergence rate manually one can choose

$$\bar{\boldsymbol{u}}_2 = \boldsymbol{B}\boldsymbol{D}^{-1}\boldsymbol{K}_p\tilde{\boldsymbol{\tau}} \tag{43}$$

instead, where $\boldsymbol{K}_p \in \mathbb{R}^{n\times n}$ can be considered as a diagonal gain matrix with constant entries. The final control law $\boldsymbol{u}_2 = \check{\boldsymbol{u}} + \bar{\boldsymbol{u}}_2$ results in the following torque dynamics

$$\dot{\tilde{\boldsymbol{\tau}}} + \boldsymbol{K}_p\tilde{\boldsymbol{\tau}} = \boldsymbol{0}, \tag{44}$$

where the convergence rate of the individual torque errors $\tilde{\boldsymbol{\tau}}_i$ depends on the corresponding entries in $\boldsymbol{K}_{p_{i,i}}$.

By exploiting the triangular system structure of the non-autonomous closed-loop systems (9),(40) and (9),(42), respectively, one can show global uniform asymptotic stability in analog fashion as has been done for the decoupling based torque controller for flexible-joint robots presented in [18].

References

[1] M. W. Spong, "Modeling and control of elastic joint robots," *Transactions of the ASME: Journal of Dynamic Systems, Measurement, and Control*, vol. 109, pp. 310–319, 1987.

[2] A. Loria and R. Ortega, "On tracking control of rigid and flexible joints robots," *Appl. Math. Comput. Sci*, vol. 5, no. 2, pp. 101–113, 1995.

[3] C. Ott, A. Albu-Schäffer, A. Kugi, and G. Hirzinger, "Decoupling based cartesian impedance control of flexible joint robots," in *Proc. IEEE Int. Conf. on Robotics and Automation*, 2003.

[4] S. Ozgoli and H. Taghirad, "A survey on the control of flexible joint robots," *Asian Journal of Control*, vol. 8, no. 4, pp. 332–344, 2006.

[5] A. De Luca and P. Lucibello, "A general algorithm for dynamic feedback linearization of robots with elastic joints," in *IEEE Int. Conf. on Robotics and Automation*, vol. 1, 1998, pp. 504–510.

[6] A. Albu-Schäffer, C. Ott, and G. Hirzinger, "A unified passivity-based control framework for position, torque and impedance control of flexible joint robots," *The International Journal of Robotics Research*, vol. 26, no. 1, pp. 23–39, 2007. [Online]. Available: http://dx.doi.org/10.1177/0278364907073776

[7] C. Ott, A. Albu-Schaffer, A. Kugi, and G. Hirzinger, "On the passivity-based impedance control of flexible joint robots," *Robotics, IEEE Transactions on*, vol. 24, no. 2, pp. 416–429, 2008.

[8] D. J. Braun, M. Howard, and S. Vijayakumar, "Exploiting variable stiffness in explosive movement tasks," in *Robotics: Science and Systems*, 2011.

[9] M. Keppler, D. Lakatos, C. Ott, and A. Albu-Schäffer, "A passivity-based controller for motion tracking and damping assignment for compliantly actuated robots," in *Decision and Control (CDC), 2016 IEEE 55th Conference on*. IEEE, 2016, pp. 1521–1528.

[10] M. Keppler, D. Lakatos, C. Ott, and A. Albu-Schäffer, "Elastic structure preserving (esp) control for compliantly actuated robots," 2018, accepted for publication in the IEEE Transactions on Robotics.

[11] ——, "Elastic structure preserving impedance (espi) control for compliantly actuated robots," 2018, submitted to IEEE Robotics and Automation Letters.

[12] A. de Luca, R. Farina, and P. Lucibello, "On the control of robots with visco-elastic joints," in *Proc. IEEE Int. Conf. on Robotics and Automation*, 2005.

[13] G. Pratt and M. Williamson, "Series elastic actuators," in *Proceedings 1995 IEEE/RSJ International Conference on Intelligent Robots and Systems. Human Robot Interaction and Cooperative Robots*. IEEE Comput. Soc. Press, 1995. [Online]. Available: http://dx.doi.org/10.1109/IROS.1995.525827

[14] F. Ghorbel, B. Srinivasan, and M. W. Spong, "On the uniform boundedness of the inertia matrix of serial robot manipulators," *Journal of Robotic Systems*, vol. 15, no. 1, 1998.

[15] W. Hahn, *Stability of Motion*. Berlin, Heidelberg: Springer Berlin Heidelberg, 1967.

[16] H. K. Khalil, *Nonlinear Systems (3rd Edition)*. Prentice Hall, 2001.

[17] J.-J. Slotine and W. Li, *Applied Nonlinear Control*. Prentice Hall, 1991.

[18] C. Ott, *Cartesian Impedance Control of Redundant and Flexible-Joint Robots*, B. Siciliano and O. Khatib, Eds. Springer, 2008.